J Appl Electrochem (2017) 47:889–903
DOI 10.1007/s10800-017-1092-z

RESEARCH ARTICLE

Electrochemistry of TiO_2/CdS composite electrodes for supercapacitor applications

P. Prasannalakshmi[1] · N. Shanmugam[1] · A. Senthil Kumar[2]

Received: 22 January 2017 / Accepted: 27 May 2017 / Published online: 5 June 2017

Abstract This paper outlines a sol–gel method for the synthesis of TiO_2/CdS composites with different CdS concentrations for use in supercapacitor applications. Composite electrodes of TiO_2/CdS containing zinc (0.25, 0.5, 0.75, and 0.1 M) and sulphide (0.5, 0.1, 1.5, and 2 M) in a 1:2 molar ratio were prepared and are labelled TC1, TC2, TC3, and TC4, respectively. The X-ray diffraction patterns displayed peaks for TiO_2 and CdS. A gradual change in morphology from rod like to spherical as the CdS content increased was observed using FE-SEM and confirmed by TEM analysis. Furthermore, the electrochemical properties of all prepared electrodes were analysed using techniques such as cyclic voltammetry (CV), galvanostatic charge–discharge (GV), electrochemical impedance spectroscopy (EIS), and cycle life testing. Among the studied electrodes, CV analysis of TC1 indicated a capacitance of 1296 Fg^{-1} at a low scan rate of 10 mVs^{-1}, whereas GV analysis showed the value to be 1320 Fg^{-1} at a scan rate of 10 Ag^{-1}. Also, the significant increase in the energy density and power density of the TC1 electrode may open a new path to supercapacitor applications. The improved electrochemical performance of TC1 can be largely attributed to its increased BET parameters, rod-like morphology, and low charge transfer resistance. Furthermore, an asymmetric capacitor (ASC) was fabricated using the TC1 electrode as the cathode material and activated carbon as the anode. The fabricated ASC had a capacitance of 685 Fg^{-1} at a scan rate of 10 Ag^{-1} with a high energy density of 219 kWh kg^{-1}. The repeatability test results imply that even after 500 cycles of operation, the as-fabricated ASC exhibits 95% capacitance retention. Additionally, on charging, the as-fabricated ASC has the ability to glow green in a light-emitting diode. Therefore, the TC1 electrode is a suitable cathode material for next-generation supercapacitors in high-energy density storage systems.

✉ N. Shanmugam
quantumgosh@rediffmail.com

[1] Department of Physics, Annamalai University, Annamalai Nagar, Chidambaram 608 002, Tamilnadu, India

[2] Nano and Bio-electrochemistry Research Laboratory, Department of Chemistry, VIT University, Vellore, Tamil Nadu, India

Graphical Abstract

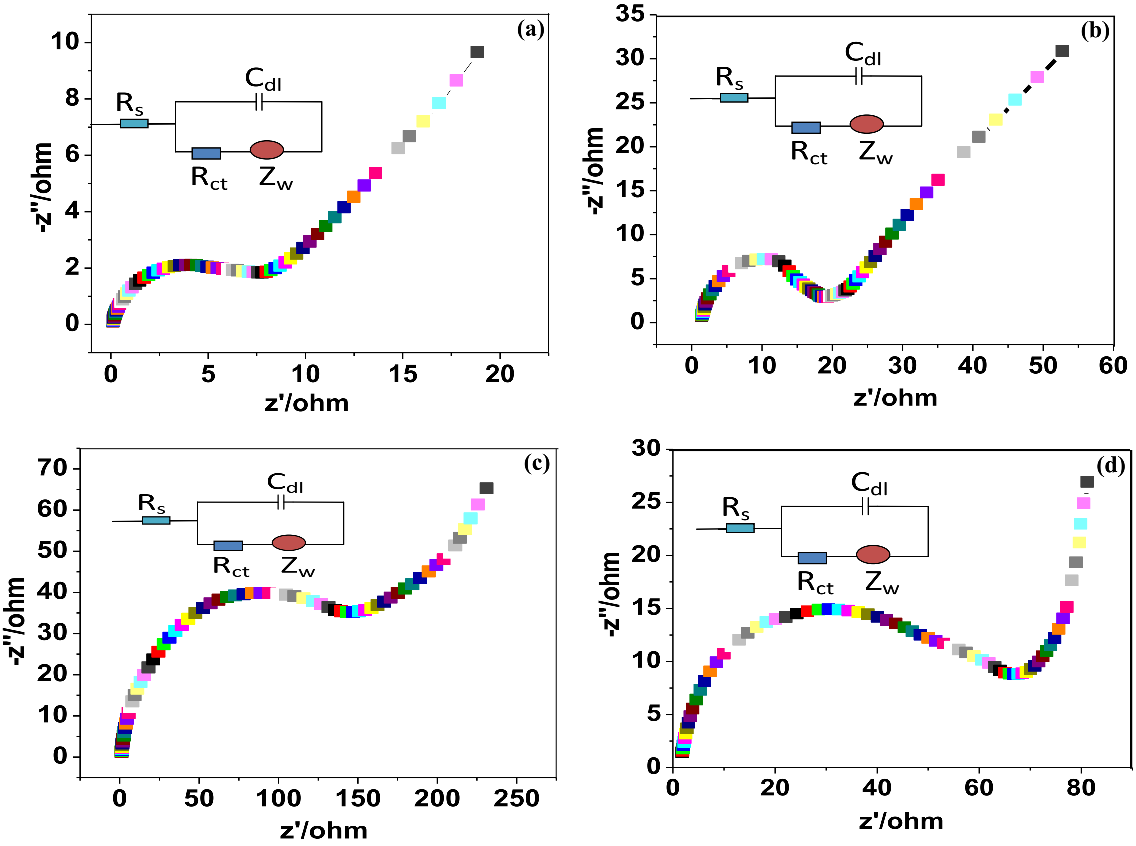

Keywords Composite · Pore size · Pseudocapacitance · Energy density · Power density

1 Introduction

Supercapacitors have greater energy discharging capabilities than conventional batteries because supercapacitors can store energy on the surface or subsurface layer of the electrode [1]. The charge storage mechanism of supercapacitors largely defines them as electric double-layer capacitors (EDLCs) and pseudocapacitors. EDLCs store charge in a non-faradaic manner, whereas pseudocapacitors adopt a faradaic mechanism [2]. Transition metal oxides play a pivotal role in energy storage. Among the transition metal oxides, the higher surface area, active electrochemical nature, and chemical stability of TiO_2 nanostructures prompt their use in energy storage applications [3]. However, portable devices require supercapacitors with higher capacitance. To achieve this, composite materials composed of transition metal oxides and metal semiconductors have recently been studied in the preparation of electrodes for energy storage applications [4–8].The energy storage capabilities of composite electrodes depend not only on the surface area but also on the morphology of the electrode [9]. Therefore, additional studies into the preparation of electrode materials for supercapacitor applications are needed. Among techniques such as sol–gel [10], spray pyrolysis [11], solvothermal [12], microwave-assisted [13], and chemical vapour deposition [14], the sol–gel technique is suitable for the preparation of TiO_2-based nanocomposites because it is performed at low temperature [15]. More recently, TiO_2-based nanocomposites have been evaluated as effective electrode materials for supercapacitor applications. Gao et al. have fabricated a multi-walled carbon nanotube–TiO_2 hybrid electrode for electrochemical capacitance applications [16]. Deshmukh et al. have reported the chemical synthesis of PANI–TiO_2 composite thin films for supercapacitor applications and achieved a capacitance of 709 Fg^{-1} [17]. The electrochemiluminescence properties of TiO_2/CdS nanocomposites have been reported by Wang et al. for use in sensing Hep G2 cells [18]. The present paper reports on the fabrication of TiO_2/CdS nanocomposites with different CdS concentrations using a sol–gel approach. The preparation procedure of the composites is shown in Scheme 1. Furthermore, the fabricated composite electrodes were studied for their

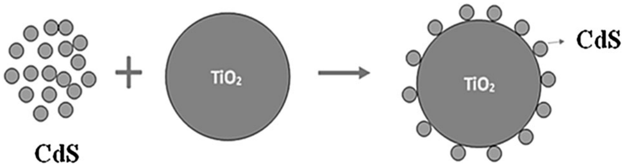

Scheme 1 The preparation procedure of TiO_2/CdS composite

suitability in supercapacitor applications using cyclic voltammetry (CV), electrochemical impedance spectroscopy (EIS), galvanostatic charge–discharge (GV), and cyclic life test. Furthermore, an asymmetric capacitor (ASC) was fabricated using the TC1 electrode as the cathode material and activated carbon as the anode. The fabricated ASC had a capacitance of 685 Fg^{-1} at a scan rate of 10 Ag^{-1} with a high energy density of 219 kWh kg^{-1}.

2 Experimental

2.1 Preparation of TiO_2/CdS nanocomposites

In the preparation of TiO_2/CdS nanocomposites, nanosized TiO_2 and CdS were prepared separately and then mixed by magnetic stirring. During the sol–gel synthesis of TiO_2, 5 ml of titanium (IV) isopropoxide was added to 50 ml of isopropyl alcohol and magnetically stirred for 20 min. Next, to initiate the ionisation of the isopropoxide chain, 20 ml of deionised water was added to the mixture. The solution was stirred for 2 h to convert the solution into a gel. Similarly, in the preparation of CdS, a 0.25 M cadmium acetate solution in 50 ml of water was magnetically stirred for 2 h with a 0.5 M sodium sulphide solution in 50 ml of water. Then, the obtained solution was poured into the prepared TiO_2 solution and magnetically stirred for

Fig. 1 XRD patterns of TiO_2/CdS nanocomposites with different CdS concentrations

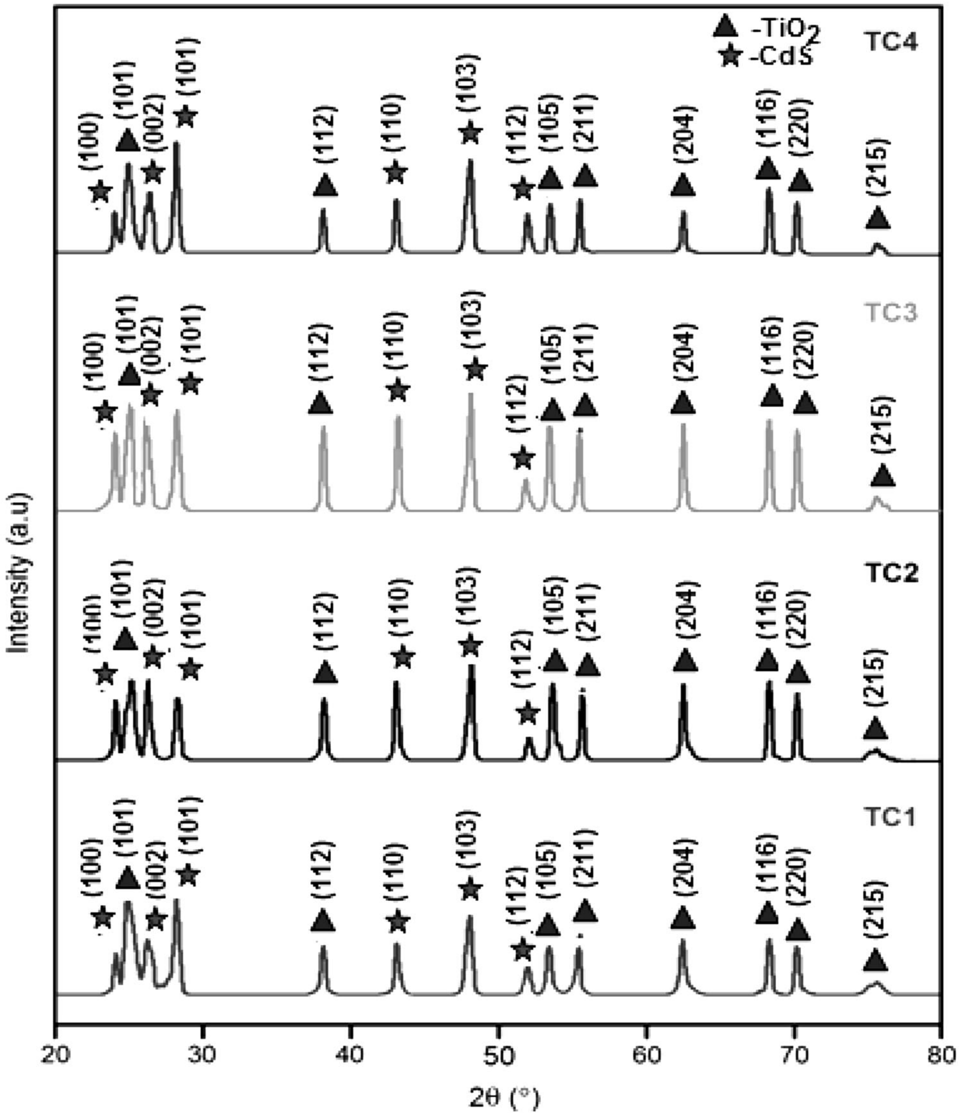

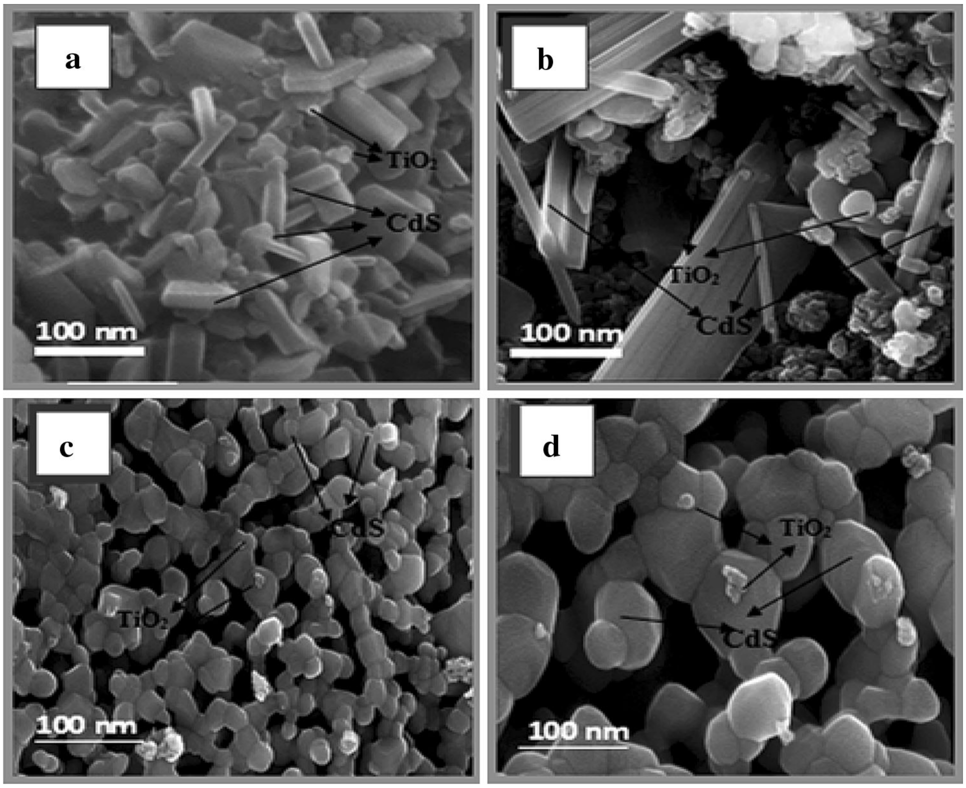

Fig. 2 FE-SEM images of **a** TC1, **b** TC2, **c** TC3, and **d** TC4

4 h to convert the solution into a gel. The prepared gel was dialysed several times with water and then dried at 100 °C for 2 h. The dried product was then annealed at 550 °C for 2 h to form the TiO_2/CdS composite. The same preparation technique was implemented for all concentrations of cadmium acetate (0.5, 0.75, and 1 M) and sodium sulphide (1, 1.5, and 2 M) in a 1:2 molar ratio. The harvested products were indexed as TC1, TC2, TC3, and TC4, respectively.

2.2 Characterisation

The diffraction patterns of the samples were recorded using an X'PERT PRO diffractometer operating at 40 kV and 20 mA using Cu Kα (1.54138 Å) radiation over the range 20–80 (2θ) at room temperature. The change in morphology on increasing CdS concentrations was observed by field emission scanning electron microscopy (FE-SEM; HITACHI S 4700) and confirmed with high-resolution scanning electron microscopy (HR-TEM; JEM-2100) analysis. The samples for morphology observation were prepared by dispersing the products in ethanol with an ultrasonic bath for 15 min and few drops of the resulting suspension into a copper grid. The BET parameters of the composites were analysed by N_2 adsorption–desorption isotherm measurements at 77 K using a Micrometrics ASAP 2010 system.

2.3 Electrochemical characterisation

Three electrodes were software controlled using a CHI 660C electrochemical workstation to analyse the electrochemical properties of the prepared electrodes. Of the three electrodes, stainless steel, Ag/AgCl, and platinum wire electrodes served as working, reference, and counter electrodes, respectively. Furthermore, the working electrode comprised an active mass of composite material (85 Wt%), carbonaceous additive (acetylene black, 10 Wt%), and 5 Wt% of Nafion binder. During the electrochemical measurements, a 0.5 M aqueous KCl solution was used as the electrolyte.

2.4 Fabrication of an asymmetric supercapacitor

To fabricate the asymmetric supercapacitor, the TiO_2/CdS cathode, activated carbon anode, and filter paper were soaked in a 0.5 M KCl solution for 24 h. Then, in the presence of the electrolyte, the soaked electrodes were stacked with the filter paper in between each layer as a separator. To avoid leakage of the electrolyte, the entire as-fabricated capacitor was encapsulated in parafilm. In the electrochemical calculations, the total mass of the electrode was used.

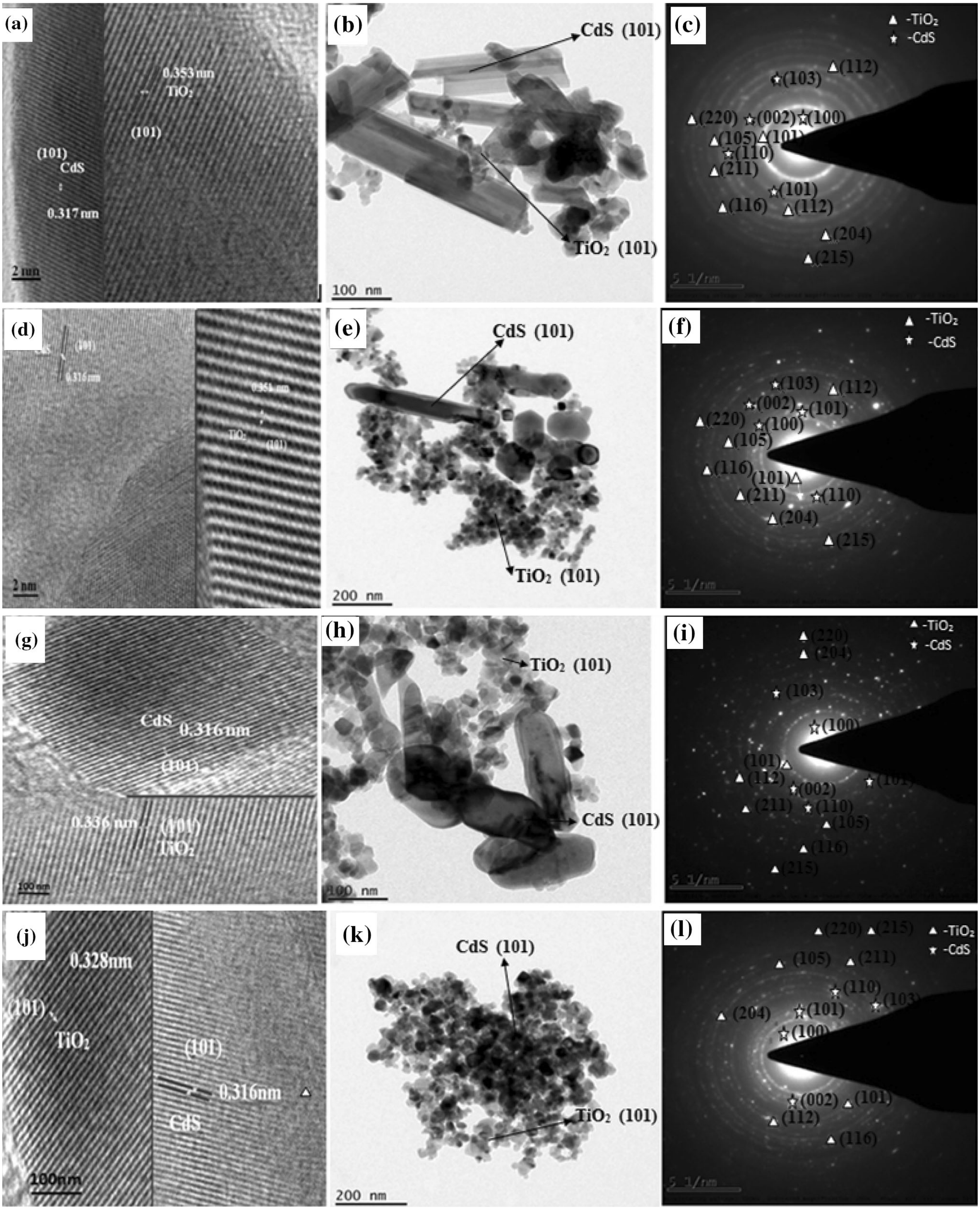

Fig. 3 HR-TEM images of TiO_2/CdS nanocomposites (**a**, **d**, **g**, **j**), corresponding TEM images (**b**, **e**, **h**, **k**), and SAED patterns (**c**, **f**, **i**, **l**)

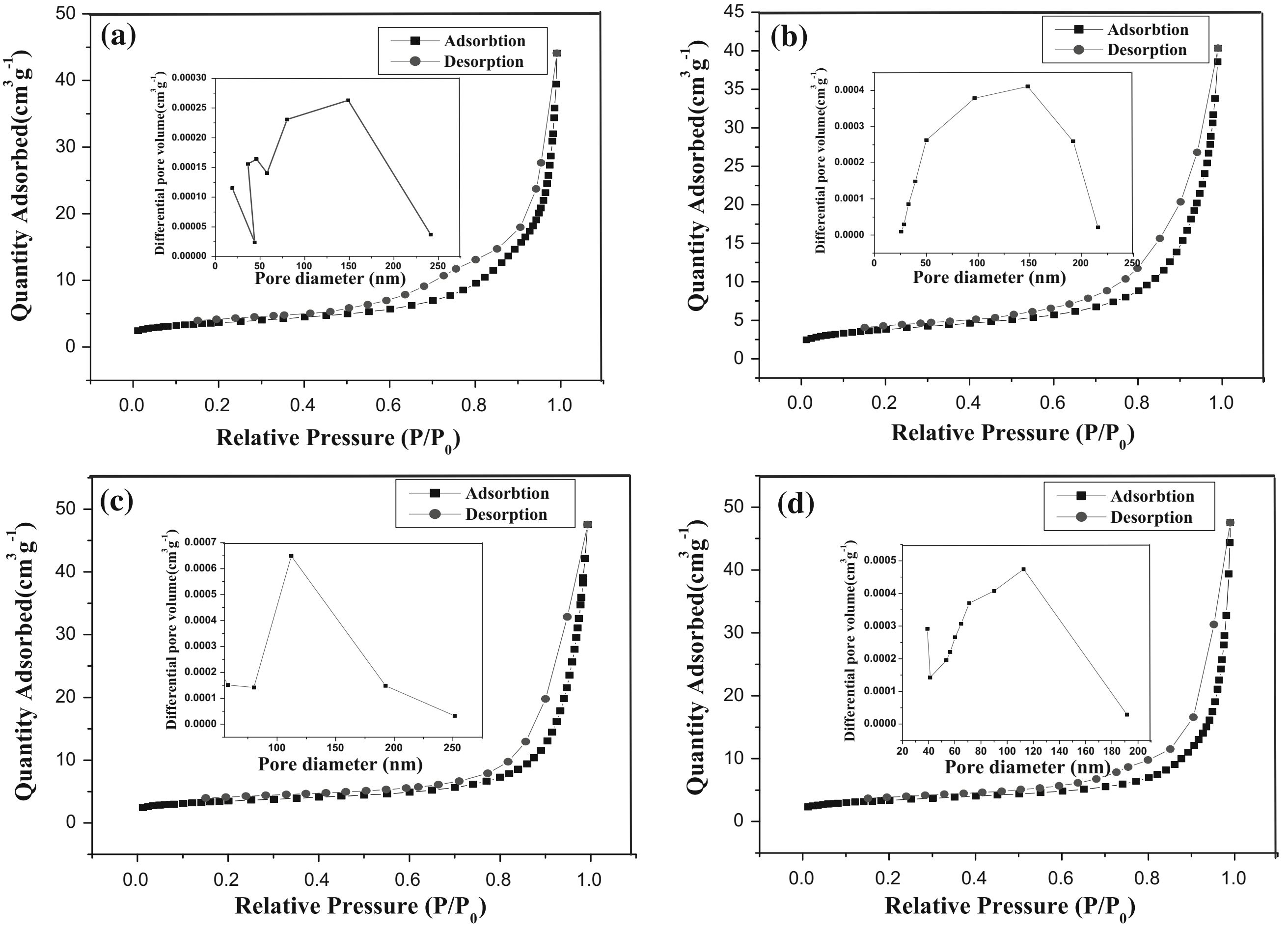

Fig. 4 N_2 adsorption–desorption isotherms of **a** TC1, **b** TC2, **c** TC3, and **d** TC4 with the corresponding pore size distribution (*insets*)

Table 1 BET parameters of TiO_2/CdS nanocomposites

Samples	S_{BET} (m^2 g^{-1})[a]	Pore size (nm)[b]	Type of hysteresis loop[c]	V_{pore} (cm^3 g^{-1})[d]
TC1	13.66	148.99	H_3	0.0736
TC2	12.93	147.79	H_3	0.0735
TC3	12.34	112.05	H_3	0.0681
TC4	11.97	102.20	H_3	0.0624

[a] Pore size estimated from differential pore volume plot

[b] BET surface area calculated from the linear part of the BET plot ($P/P_0 = 11.97$–13.66 m^2 g^{-1})

[c] Type of hysteresis loop as specified in the IUPAC manual

[d] Total pore volume determined from the volume of N_2 adsorbed at about $P/P_0 = 0.9901$ (cm^3 g^{-1})

3 Result and discussion

3.1 X-ray diffraction

X-ray diffraction profiles of the TiO_2/CdS nanocomposites were recorded in the 2θ range between 20° and 80° and are presented in Fig. 1. All of the diffraction results show sharp diffraction peaks due to reflections from the (101), (112), (105), (211), (204), (116), (220), and (215) planes of anatase TiO_2 (JCPDS No: 89-4921) and the (100), (002), (101), (110), (103), and (112) planes of hexagonal CdS (JCPDS No: 41-1049), confirming the co-existence of both TiO_2 and CdS in the prepared nanocomposites. The diffraction peaks observed in the present study match exactly the results reported previously by other research groups [19–21]. Increasing CdS content caused a significant enhancement in the intensity of the CdS peaks in the diffraction patterns.

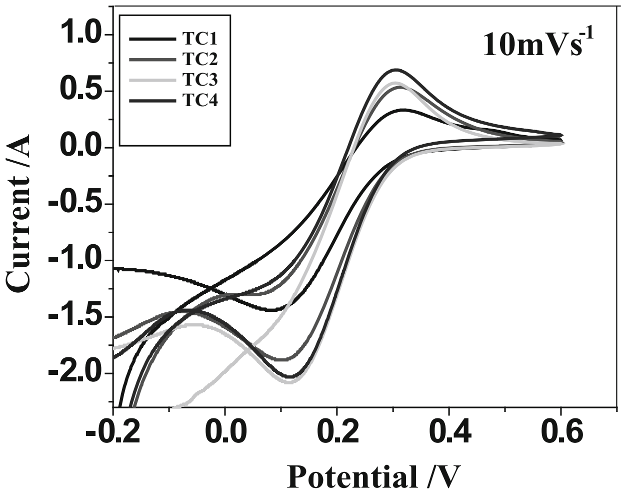

Fig. 5 Cyclic voltammograms for TiO_2/CdS composites at a scan rate of 10 mVs^{-1}

3.2 Morphological analysis

In tailoring the morphologies of the composites, CdS content plays an important role. The morphologies of the composites were studied by FE-SEM analysis and Fig. 2a–d depicts the FE-SEM micrographs of TiO_2/CdS nanocomposites with different CdS loadings. As shown in Fig. 2a, the TC1 sample exhibits a rod-like morphology. As the CdS content increases, the composites TC2 and TC3 reveal the presence of irregular particles along with some remaining rod-shaped particles (Fig. 2b, c). However, at higher CdS loadings, the morphology of TC4 completely changes from rod like to spherical (Fig. 2d). The composite morphologies were further confirmed by TEM analysis. Figure 3 depicts the TEM results of the composites. As shown in Fig. 3a, the HR-TEM image of the TC1 sample consists of well-ordered crystalline (101) planes of TiO_2 and CdS with spacings of 0.353 and 0.317 nm, respectively. The corresponding SAED pattern reveals the existence of well-established diffraction rings of TiO_2 and CdS, indicating highly ordered subunits in the composite (Fig. 3c). The TEM micrograph of TC1 reveals that nanosized TiO_2 is uniformly surrounded by CdS and has a one-dimensional, rod-like morphology (Fig. 3b). A similar rod-like morphology was reported by Jia et al. for TiO_2@CdS nanocomposites [22]. As the CdS content increases in TC2, TC3, and TC4, CdS layers establish themselves around TiO_2, as shown in the HR-TEM images (Fig. 3d, g, j). Furthermore, the corresponding SAED patterns also show the existence of intense concentric diffraction rings of CdS among the diffraction rings of TiO_2 (Fig. 3f, i, l). However, the TEM micrographs show a gradual change in morphology from rod like to spherical as the concentration of CdS increases (Fig. 3e, h, k). The results of the TEM analysis exactly match the variation in morphology of the composites observed by FE-SEM.

3.3 BET surface area measurement

N_2 adsorption–desorption isotherms of the electrodes are presented in Fig. 4a–d with the insets showing pore size distributions. Notably, all of the observed patterns show type IV curves accompanied by type H_3 hysteresis loops, confirming the presence of a mesoporous structure [23]. Table 1 lists the surface areas, pore sizes, and pore volumes of the samples derived from the respective adsorption–desorption curves. It is easily observed that among the studied composites TC1 exhibits the highest surface area at 13.66 $m^2\ g^{-1}$ with a pore size and a pore volume of 148.99 nm and 0.0736 $cm^3\ g^{-1}$, respectively. The higher surface area, pore size, and pore volume of the sample may improve the electrode–electrolyte interaction to result in improved capacitance behaviour. As the CdS content increases, BET-related parameters decrease. Therefore, TC1 is expected to have superior electrochemical activity compared with the other prepared composites.

3.4 Cyclic voltammetry analysis

Cyclic voltammetry can provide sufficient information regarding the suitability of the electrode materials for supercapacitor applications. Figure 5 shows the CV curves of the electrodes taken at a scan rate of 10 mVs^{-1} in the potential range of −0.2 to +0.6 V using a 0.5 M KCl electrolyte solution. As depicted in the figure, all of the

Table 2 Cyclic voltammogram mediated capacitance of TiO_2/CdS electrode at different scan rates

Electrode	Capacitance C_s (Fg^{-1})									
	Scan rate (mVs^{-1})									
	10	20	40	60	80	100	200	300	400	500
TC1	1296	542	262	164	129	105	51	34	28	20
TC2	1186	534	251	169	125	101	49	33	27	21
TC3	1113	565	285	192	139	116	55	37	30	22
TC4	893	428	192	111	84	67	36	18	17	14

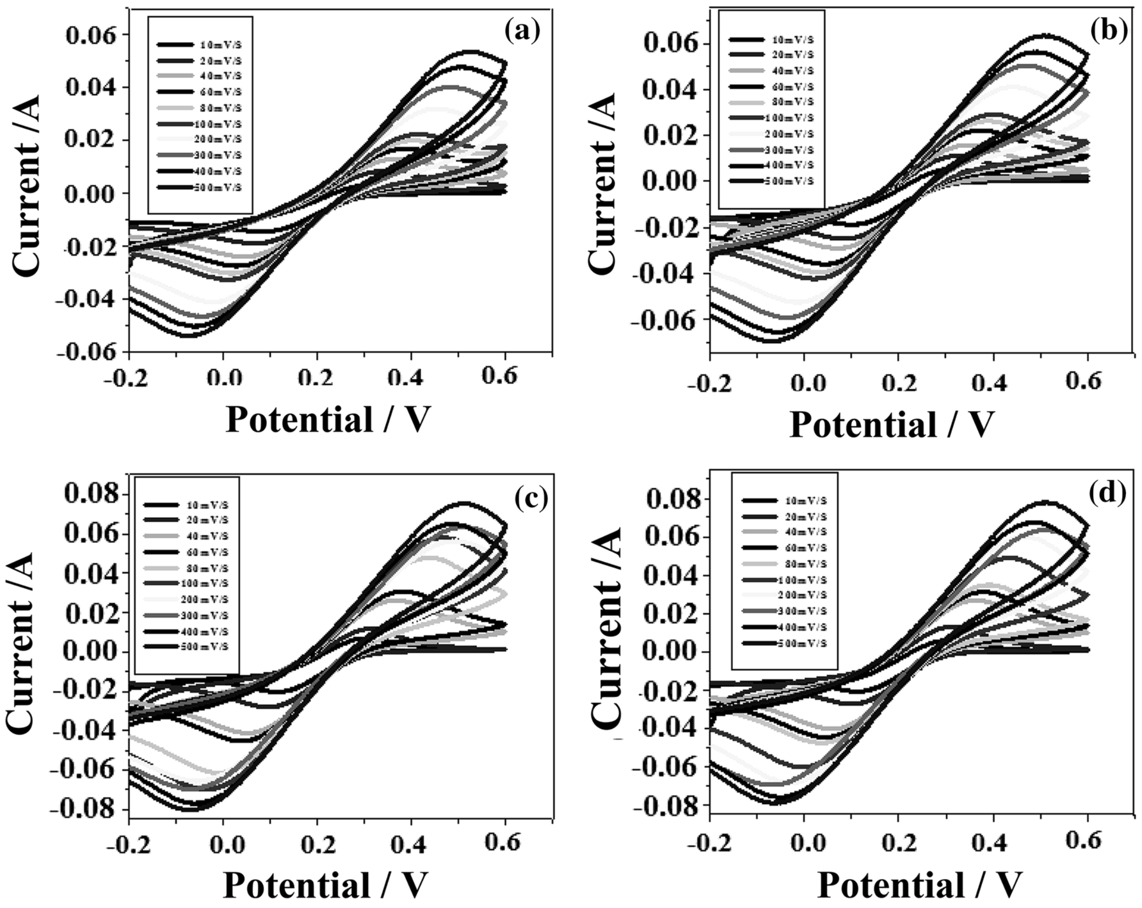

Fig. 6 Cyclic voltammogram performance of **a** TC1, **b** TC2, **c** TC3, and **d** TC4 at different scan rates

curves show a pair of redox peaks, indicating the pseudocapacitance of the prepared electrodes [24]. Interestingly, as CdS content increases, the intensities of the redox peaks increase, as the smaller band gap of CdS may cause CdS to receive more electrons from the electrolyte solution that are then transferred to the wide-band gap material TiO_2 [25]. The specific capacitance of the electrodes was calculated using the usual formula [26], and the results are shown in Table 2. Among the studied electrodes, the highest capacitance value of 1296 Fg^{-1} was recorded for TC1, whereas the TC2, TC3, and TC4 electrodes exhibited the capacitance values of 1086, 930, and 893 Fg^{-1}, respectively. The capacitances recorded in the present study are greater than the values reported for TiO_2-based nanocomposites by other researchers [27–29]. The outstanding capacitance of TC1 originates from its increased BET parameters, rod-like morphology, and low charge transfer resistance. An electrode with a high BET surface area has an enhanced probability for electrode/electrolyte interaction. Furthermore, the microporous structure and low charge transfer resistance may accelerate the penetration of K^+ ions from the electrolyte to result in an enhanced rate of K^+ insertion and exertion [30]. In addition, the rod-like morphology of TC1 may provide a short diffusion path for both ions and electrons, leading to higher charge–discharge rates. To determine the effect of scan rate on the capacitance behaviour, CV measurements were performed at different scan rates (10–500 mVs^{-1}), and the results are presented in Fig. 6a–d. At high scan rates, as a result of a higher degree of electric polarisation and irreversible reactions, the cathodic and anodic peaks shift to higher and lower potentials, respectively [31]. The capacitance response of the electrodes on different scan rates was estimated, and the values are presented in Table 2. From the table, it is clear that the capacitance decreases with increasing scan rate. A potential explanation may be that at high scan rates the inner active sites of the electrodes are not involved in the insertion reaction, which in turn reduces capacitance [32].

3.5 Electrochemical impedance spectroscopy

Electrochemical impedance spectroscopy (EIS) is a versatile tool for evaluating the charge storage capability of capacitors [33]. Figure 7a–d depicts the recorded EIS curves of the composites with different CdS concentrations

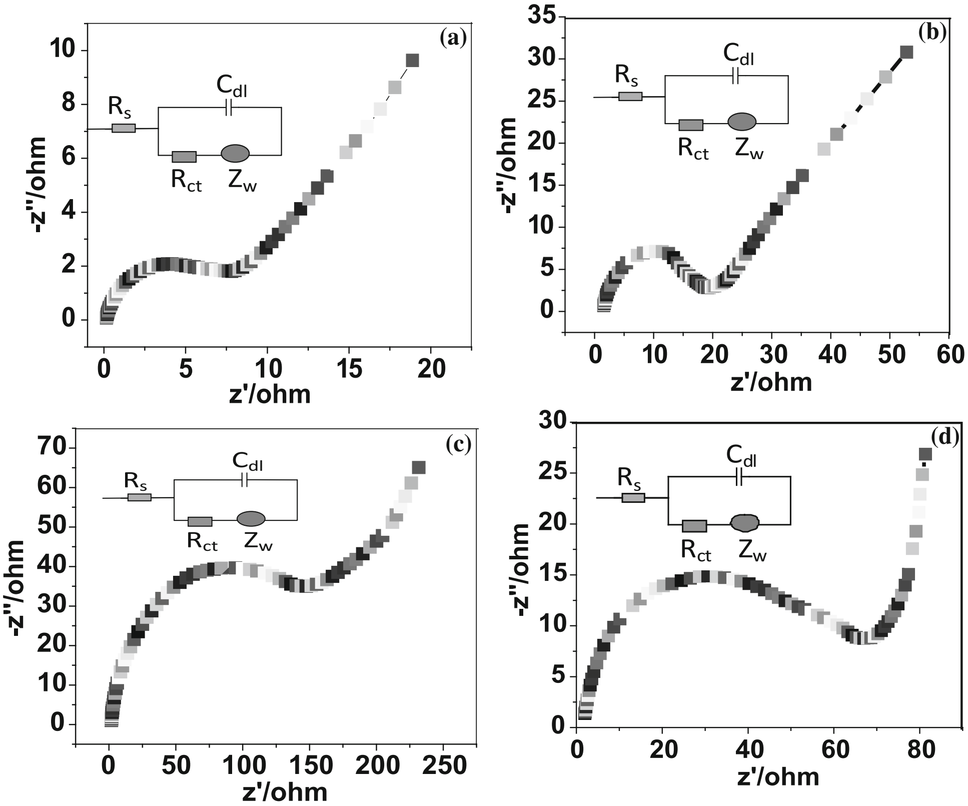

Fig. 7 EIS spectra (Nyquist plot) of **a** TC1, **b** TC2, **c** TC3, and **d** TC4 with electrical equivalent circuit (*inset*)

Table 3 EIS parameters of TiO_2/CdS electrodes

Electrode	R_s (Ohm)	C_{dl} (μF)	R_{ct} (Ohm)
TC1	0.07	714	7.33
TC2	0.87	640	17
TC3	1.27	179	63
TC4	2	105	139

at an open circuit potential of 100 mV. It can be seen that all samples exhibit a semicircle initiating from the high-frequency region, followed by a linear portion. Usually, the diameter of the semicircle determines the value of the charge transfer resistance (R_{ct}), whereas the linear portion implies a diffusion process [34]. In the present study, the diameter of the semicircle increases with increasing CdS content, revealing hindered electron transfer at higher CdS content. The insets of Fig. 7a–d display the equivalent circuits of the EIS data, showing the charge transfer resistance (R_{ct}), double-layer capacitance (C_{dl}), and Warburg impedance (Z_w). The estimated parameters are presented in Table 3. From the table, it is evident that, compared with other electrodes, TC1 exhibits a low charge transfer resistance of 7.22 Ohm, a low solution resistance of 0.07 Ohm, and a higher C_{dl} value of 714 μF, suggesting its use as an electrode material in supercapacitor applications. The potential causes of low charge transfer resistance in TC1 are the high BET surface area and 1D morphology. Wei et al. reported a similar type of low charge transfer resistance behaviour in CdS-modified, 1D TiO_2 nanofibres [35]. Furthermore, the value of R_{ct} observed in the present study is less than the value of 62 Ohm reported by Li et al. for Cd-doped TiO_2 nanorod arrays [36]. Pawar et al. have reported a charge transfer resistance of 14,210 Ohm for a TiO_2/CdS photoanode [37].

3.6 Galvanostatic charge–discharge analysis

The galvanostatic charge–discharge measurements of the electrodes were recorded at different current densities (10–50 Ag^{-1}) in the potential range of −0.2 to +0.6 V as shown in Fig. 8a–d. Irrespective of current density, symmetrical curves were observed for all electrodes, despite the fact that discharge time decreased as current density increased. The specific capacitance of the samples was estimated from the GV curves using the formula [38]:

$$C = \frac{I \times \Delta t}{\Delta V \times m},$$

where C (Fg^{-1}) is the specific capacitance, Δt (s) is the discharge time, ΔV (V) is the potential window, and m (g) is the mass of the active material.

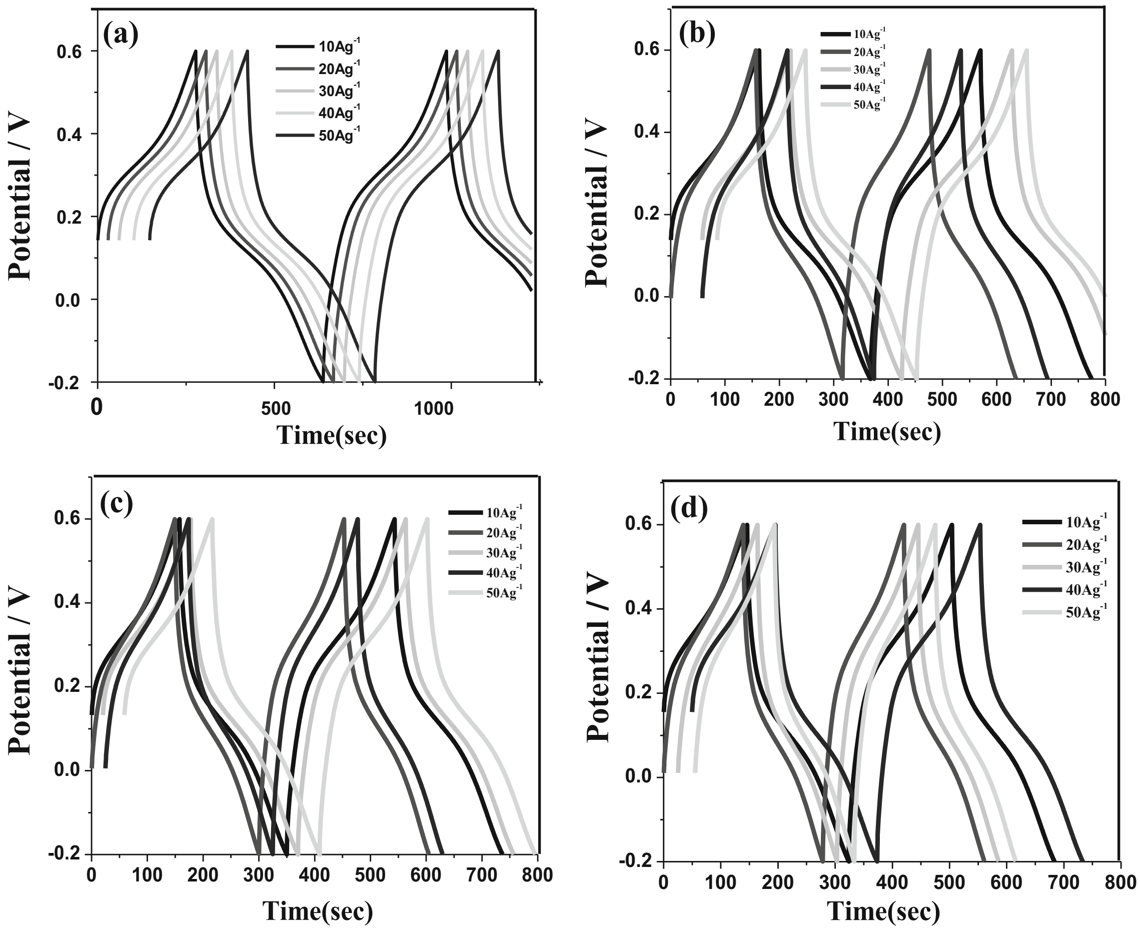

Fig. 8 Galvanostatic charge–discharge performances of **a** TC1, **b** TC2, **c** TC3, and **d** TC4 at different scan rates

Table 4 depicts the variation in capacitance with respect to current density. At a low scan rate of 10 Ag^{-1}, the highest capacitance at 1320 Fg^{-1} was recorded for the TC1 electrode, and moreover the TC1 electrode exhibited higher capacitance values over the entire range of current densities. The capacitance values derived from GV analysis are similar to the values determined by CV analysis. Indeed, the reliability of a capacitor is largely estimated from the energy density and current density, which are estimated from the following equations [39]:

$$E = \frac{1}{2} C\,(\Delta V)^2$$

$$P = \frac{E}{\Delta t},$$

where P (kW kg^{-1}) is the power density, C (Fg^{-1}) is the specific capacitance, ΔV (V) is the potential window of the discharge process, Δt (s) is the discharge time, and E (kWh kg^{-1}) is the energy density.

Strikingly, the TC1 electrode possesses higher energy density and power density over the entire range of current densities (Table 4), making it especially suitable for supercapacitor applications. Moreover, the rod-like morphology produces a more active surface for the diffusion of both electrons and ions, and the low charge resistance increases the permeability of the charge carriers, which are prime factors in the improvement of capacitance.

3.7 Cycle life test

A cycle life test was conducted to analyse the reliability of the electrodes in capacitor applications. Figure 9 presents the relation between the specific capacitance of the electrodes and the cycle number recorded at a current density of 10 Ag^{-1}. It is obvious that all of the electrodes have absolute cyclic activity even after 500 cycles of operation, with nearly 99% retention of capacitance. Furthermore, the appearance of symmetry between the charge and discharge

Table 4 Galvanostatic charge–discharge capacitance, energy density, and power density of TiO_2/CdS electrodes at different scan rates (10–50 Ag^{-1})

Electrode	TC1					TC2					TC3					TC4				
Scan rates (Ag^{-1})	10	20	30	40	50	10	20	30	40	50	10	20	30	40	50	10	20	30	40	50
Capacitance C_s (Fg^{-1})	1320	1240	1200	1180	1150	860	810	804	769	652	854	807	801	667	651	738	651	587	574	572
Energy density (kWh kg^{-1})	486	478	384	377	368	275	259	257	246	208	273	251	250	213	206	243	236	187	183	182
Power density (kW kg^{-1})	4800	4860	5311	5385	6133	4790	4820	4828	4829	4830	4770	4810	4820	4825	4827	4769	4790	4810	4816	4860

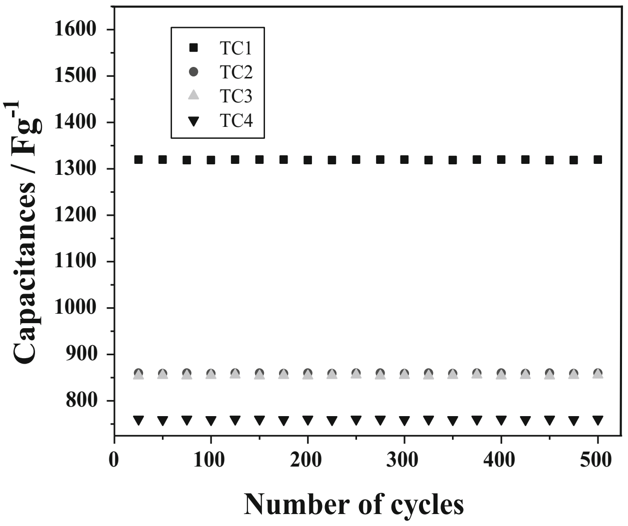

Fig. 9 Cyclic test performance of TiO_2/CdS electrodes at a current density of 10 Ag^{-1}

curves for the last 20 cycles confirm the stability of the capacitance activity of the prepared electrodes (Fig. 10).

3.8 Energy storage ability of the as-fabricated ASC

To test the reliability of the TiO_2/CdS electrode for practical usage, an asymmetric supercapacitor (ASC) device was fabricated using the TC1 electrode as the cathode, activated carbon (AC) as the anode, and a piece of filter paper as the separator. The as-fabricated device is shown in Fig. 11a, b. To study the charge storage ability of the as-fabricated ASC, CV and GV analyses were performed for activated carbon and the ASC. Figure 12a illustrates the CV responses of activated carbon (AC) recorded at different scan rates in 0.5 M KCl electrolyte. As indexed in the figure, all of the curves show a rectangular shape, indicating the electric double-layer capacitance (EDLC) nature of the electrode. However, at high scan rates, deviation in the rectangular shape was observed. The CV curves of the as-fabricated ASC show the presence of a couple of redox peaks, revealing the pseudocapacitance nature of the ASC (Fig. 12b). Furthermore, to evaluate the values of the energy density and power density, GV curves were recorded for both AC and the ASC at different scan rates (10–50 Ag^{-1}), and the results are presented in Fig. 12c and d, respectively. As shown in the figures, all of the curves exhibit an almost triangular shape, revealing the suitability of the ASC for supercapacitor applications. The specific capacitance values of AC and the ASC were estimated from the usual formula and are presented in Table 4. As indexed in the table, AC has a capacitance of 258 Fg^{-1} at 10 Ag^{-1}, whereas the value was 685 Fg^{-1} for the ASC.

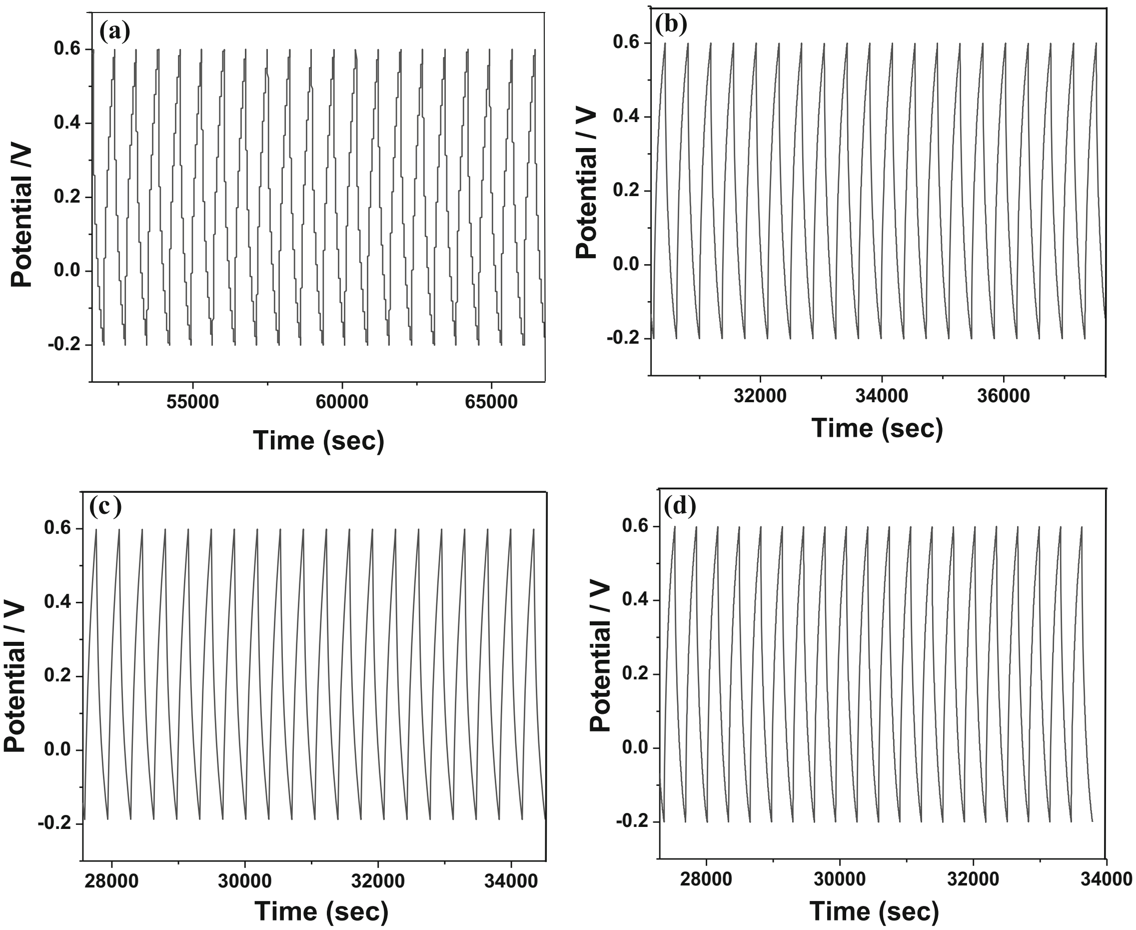

Fig. 10 Charge–discharge curves of **a** TC1, **b** TC2, **c** TC3, and **d** TC4 electrodes for the last 20 cycles

Fig. 11 **a** Schematic illustration of the as-fabricated TC1 device. **b** A simple application in a commercial light-emitting diode (LED)

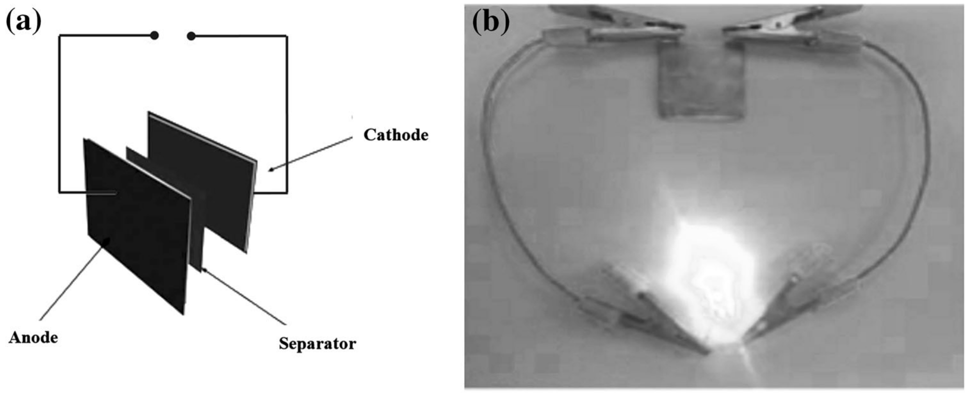

Furthermore, the energy density and power density were calculated for AC and the ASC, and the obtained values are included in Table 4. It was observed that at a scan rate of 10 Ag^{-1}, AC has an energy density and a power density of 82 kWh kg^{-1} and 630 kW kg^{-1}, whereas the values are 219 kWh kg^{-1} and 4860 kW kg^{-1} for the ASC, respectively. The energy density and power density of the present as-fabricated ASC are greater than those reported by other research groups [6, 40]. In addition, a cycle life test for the ASC was carried out for 500 cycles, and the results show that even after 500 cycles of operation the as-fabricated ASC exhibits 95% capacitance retention (Fig. 12e). Using the as-fabricated ASC, we succeeded in lighting a commercial light-emitting diode (Fig. 12b).

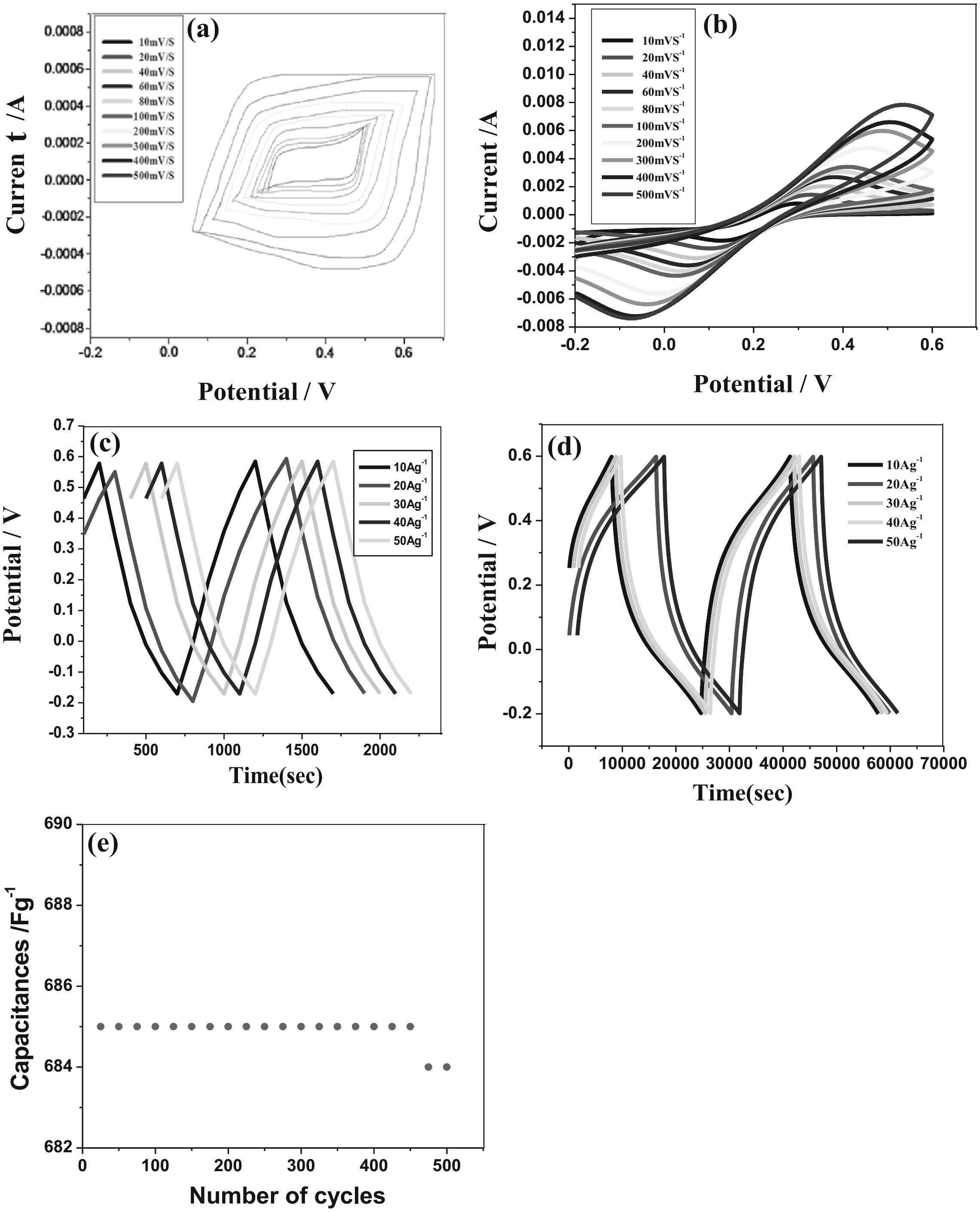

Fig. 12 **a** CV curves of AC, **b** CV curves of the as-fabricated ASC, **c** GV curves of AC, **d** GV curves of the as-fabricated ASC, and **e** cycle test performance of the ASC

4 Summary and conclusions

A sol–gel approach was used to fabricate TiO_2/CdS electrodes with different CdS concentrations in order to determine their suitability for supercapacitor applications. The diffraction patterns of the products show peaks for TiO_2 and CdS with no other impurities, revealing that the prepared products consist purely of TiO_2/CdS composites. A morphology transformation from rod like to spherical was observed using FE-SEM and confirmed by TEM micrographs. Furthermore, the analysed electrochemical properties suggest that among the studied electrodes the

TC1 electrode is the most suitable for supercapacitor applications due to its superior specific capacitance, energy density, and power density. The enhanced electrochemical properties of the electrode originate from its increased BET parameters, rod-like morphology, and low charge transfer resistance. Furthermore, as a practical application, using the TC1 electrode, an asymmetric capacitor was fabricated. The as-fabricated ASC delivered high energy density (219 kWh kg^{-1}) and power density (4860 kW kg^{-1}) with 95% capacitance retention. The present investigation strongly suggests the usage of TiO_2/CdS composites as electrode materials in next-generation pseudocapacitors.

Acknowledgements The authors wish to thank Dr. V. Ramaswamy, Professor and Head, Department of Physics, Annamalai University, for providing necessary facilities to carry out this work.

References

1. Zhang Q, Uchaker E, Candelaria SL, Cao G (2013) Nanomaterials for energy conversion and storage. Chem Soc Rev 42(7):3127–3171
2. Narayanan R, Kumar PN, Deepa M, Srivastava AK (2015) Combining energy conversion and storage: a solar powered supercapacitor. Electrochim Acta 178:113–126
3. Xia X, Luo J, Zeng Z, Guan C, Zhang Y, Tu J, Zhang H, Fan HJ (2012) Integrated photoelectrochemical energy storage: solar hydrogen generation and supercapacitor. Sci Rep. 2:981–987
4. Long X, Wang Z, Xiao S, An Y, Yang S (2016) Transition metal based layered double hydroxides tailored for energy conversion and storage. Mater Today 19(4):213–226
5. Chen D, Wang Q, Wang R, Shen G (2015) Ternary oxide nanostructured materials for supercapacitors: a review. J Mater Chem A. 3(19):10158–10173
6. Wang YG, Wang ZD, Xia YY (2005) An asymmetric supercapacitor using RuO_2/TiO_2 nanotube composite and activated carbon electrodes. Electrochim Acta 50:5641–5646
7. Zhu DD, Wang YD, Yuan GL, Xia H (2014) High-performance supercapacitor electrodes based on hierarchical Ti@MnO_2 nanowire arrays. Chem Commun. 50:2876–2878
8. Kim J-H, Zhu K, Yan Y, Perkins CL, Frank AJ (2010) Microstructure and pseudocapacitive properties of electrodes constructed of oriented NiO–TiO_2 nanotube arrays. Nano Lett 10:4099–4104
9. Wang G, Zhang L, Zhang J (2012) A review of electrode materials for electrochemical supercapacitors. Chem Soc Rev 41(2):797–828
10. Epifani M, Chávez-Capilla T, Andreu T, Arbiol J, Palma J, Morante JR, Díaz R (2012) Surface modification of metal oxide nanocrystals for improved supercapacitors. Energy Environ Sci 5(6):7555–7558
11. Shin K, Im SH, Yoo PJ, Kim D, Park JH (2010) CdS or CdSe decorated TiO_2 nanotube arrays from spray pyrolysis deposition: use in photoelectrochemical cells. Chem Commun. 46:2385–2387
12. Nam CT, Falconer JL, Du LM, Yang WD (2014) Morphology, structure and adsorption of titanate nanotubes prepared using a solvothermal method. Mater Res Bull 51:49–55
13. Hu CC, Yang YL, Lee TC (2010) Microwave-assisted hydrothermal synthesis of $RuO_2{\cdot}xH_2O$–TiO_2 nanocomposites for high power supercapacitors. Electrochem Solid State Lett. 13(12):A173–A176
14. Du J, Gu X, Guo HZ, Liu J, Wu Q, Zou JG (2015) Self-induced preparation of TiO_2 nanowires by chemical vapor deposition. J Cryst Growth 427:54–59
15. Katoch A, Burkhart M, Hwang T, Kim SS (2012) Synthesis of polyaniline/TiO_2 hybrid nanoplates via a sol–gel chemical method. Chem Eng J. 192:262–268
16. Gao Z, Cui Z, Zhu S, Liang Y, Li Z, Yang X (2015) Design and synthesis of MWNTs–TiO_2 nanotube hybrid electrode and its supercapacitance performance. J Power Source. 283:397–407
17. Deshmukh PR, Patil SV, Bulakhe RN, Pusawale SN, Shim JJ, Lokhande CD (2015) Chemical synthesis of PANI–TiO_2 composite thin film for supercapacitor application. RSC Adv. 5(84):68939–68946
18. Wang L, Ma S, Wang X, Liu D, Liu S, Han X (2013) Electrochemiluminescent TiO_2/CdS nanocomposites for efficient immunosensing of $HepG_2$ cells. J Mater Chem B. 1(38):5021–5027
19. Ghows N, Entezari MH (2012) Sono-synthesis of core–shell nanocrystal (CdS/TiO_2) without surfactant. Ultrason Sonochem. 19(5):1070–1078
20. Liu S, Zhang N, Tang ZR, Xu YJ (2012) Synthesis of one-dimensional CdS@ TiO_2 core–shell nanocomposites photocatalyst for selective redox: the dual role of TiO_2 shell. ACS Appl Mater Interfaces. 4:6378–6385
21. Datta A, Panda SK, Chaudhuri S (2007) Synthesis and optical and electrical properties of CdS/ZnS core/shell nanorods. J Phys Chem C. 111(46):17260–17264
22. Jia H, Xu H, Hu Y, Tang Y, Zhang L (2007) TiO_2@ CdS core–shell nanorods films: fabrication and dramatically enhanced photoelectrochemical properties. Electrochem Commun. 9:354–360
23. Li GS, Zhang DQ, Yu JC (2009) A new visible-light photocatalyst: CdS quantum dots embedded mesoporous TiO_2. Environ Sci Technol. 43:7079–7085
24. Patil UM, Gurav KV, Fulari VJ, Lokhande CD, Joo OS (2009) Characterization of honeycomb-like "β-Ni $(OH)_2$" thin films synthesized by chemical bath deposition method and their supercapacitor application. J Power Sources. 188:338–342
25. Tian CY, Zhao WW, Wang J, Xu JJ, Chen HY (2012) Amplified quenching of electrochemiluminescence from CdS sensitized TiO_2 nanotubes by CdTe–carbon nanotube composite for detection of prostate protein antigen in serum. Analyst. 137:3070–3075
26. Dubal DP, Kim WB, Lokhande CD (2012) Galvanostatically deposited Fe: MnO_2 electrodes for supercapacitor application. J Phys Chem Solids 73:18–24
27. Ke Q, Zheng M, Liu H, Guan C, Mao L, Wang J (2015) Sci Rep. 10:13940–13946
28. Kim HI, Kim HJ, Morita M, Park SG (2010) Preparation and electrochemical performance of CNT electrode with deposited titanium dioxide for electrochemical capacitor. Bull Korean Chem Soc. 31:423–428
29. Zhang B, Shi R, Zhang Y, Pan C (2013) CNTs/TiO_2 composites and its electrochemical properties after UV light irradiation. Prog Nat Sci Mater Int. 23(2):164–169
30. Luo G, Shen K, Zheng J, Xu C (2016) CdS modified TiO_2 films showing multicolor switching and enhanced optical contrast. J Mater Chem C. 4:9085–9093
31. Yang S, Wu X, Chen C, Dong H, Hu W, Wang X (2012) Spherical α-Ni $(OH)_2$ nanoarchitecture grown on graphene as advanced electrochemical pseudocapacitor materials. Chem Commun. 48:2773–2775

32. Gobal F, Faraji M (2015) Electrochemical synthesis of reduced graphene oxide/TiO_2 nanotubes/Ti for high-performance supercapacitors. Ionics. 21(2):525–531
33. Huang J, Li Z, Liaw BY, Zhang J (2016) Graphical analysis of electrochemical impedance spectroscopy data in Bode and Nyquist representations. J Power Sources. 309:82–98
34. Li F, Yu Y, Cui H, Yang D, Bian Z (2013) Label-free electrochemiluminescence immunosensor for cardiac troponin I using luminol functionalized gold nanoparticles as a sensing platform. Analyst 138:1844–1850
35. Wei Z, Li Y, Luo S, Liu C, Meng D, Ding M, Zeng G (2014) Hierarchical heterostructure of CdS nanoparticles sensitized electrospun TiO_2 nanofibers with enhanced photocatalytic activity. Sep Purif Technol. 122:60–66
36. Li Y, Guo Y, Li Y, Zhou X (2016) Fabrication of Cd-Doped TiO_2 nanorod arrays and photovoltaic property in perovskite solar cell. Electrochimica Acta. 200:29–36
37. Pawar SA, Patil DS, Lokhande AC, Gang MG, Shin JC, Patil PS, Kim JH (2016) Chemical synthesis of CdS onto TiO_2 nanorods for quantum dot sensitized solar cells. Opt Mater. 58:46–50
38. Mehar SK, RengaRao G (2011) Ultralayered Co_3O_4 for high-performance supercapacitor applications. J Phys Chem 115:15646–15654
39. Luo Y, Kong D, Luo J, Chen S, Zhang D, Qiu K, Qi X, Zhang H, Li CM, Yu T (2013) Hierarchical TiO_2 nanobelts@MnO_2 ultrathin nanoflakes core–shell array electrode materials for supercapacitors. RSC Adv. 3:14413–14422
40. Lu X (2013) H-TiO_2@MnO_2//H-TiO_2@C core-shell nanowires for high performance and flexible asymmetric supercapacitors. Adv Mater 25:267–272